A Direct Maximum Power Point Tracking Method for Single-Phase Grid-Connected PV Inverters

Faicel El Aamri, Hattab Maker, Dezso Sera, *Senior Member, IEEE*, Sergiu Viorel Spataru, Josep M. Guerrero, *Fellow, IEEE*, and Azeddine Mouhsen

***Abstract*—A direct maximum power point tracking (MPPT) method for PV systems has been proposed in this work. This method solves two of the main drawbacks of the perturb and observe MPPT, namely: 1) the tradeoff between the speed and the oscillations in steady-state and 2) the poor effectiveness in dynamic conditions, especially in low irradiance when the measurement of signals becomes more sensitive to noise. The proposed MPPT is designed for single-phase single-stage grid-connected PV inverters and is based on estimating the ripple of the instantaneous PV power and voltage, using a second-order generalized integrator-based quadrature signal generator. We analyzed the global stability of the closed-loop control system and validated the proposed algorithm through simulation and experiments on an inverter test platform according to the EN 50530 standard. The experimental results confirm the performance of the proposed method in terms of both speed and tracking efficiency.**

***Index Terms*—EN 50530 standard, Lyapunov stability, maximum power point tracking (MPPT), perturb and observe (P&O), single-stage PV inverter.**

I. Introduction

ONE crucial component of the control system of any PV inverter is the maximum power point tracking (MPPT) algorithm, which controls the inverter power extraction and operation on the PV array's nonlinear current-voltage (I-V) characteristic curve. As an added complexity, the PV array's I-V characteristic is highly dependent on the incident solar irradiance and cell temperature. Therefore, fast changes in irradiance conditions due to moving clouds, cause fast changes in the maximum power point location on the I-V curve, which requires an efficient MPPT algorithm [1]–[3].

The perturb and observe (P&O) is one of the most popular MPPT algorithms, due to its simplicity, ease of implementation, and because it does not require any information about the PV array [4]. The basic algorithm uses a fixed voltage step to increase or decrease the PV array voltage, afterwards, the algorithm compares the current PV array power ($P_{\rm pv}[k]$), with its previous value, where $\Delta P = P_{\rm pv}[k] - P_{\rm pv}[k-1]$. If the power increases $\Delta P > 0$, the algorithm continues to perturb the system in the same direction, alternatively if the power decreases $\Delta P < 0$, the system will be perturbed in the opposite direction. This process is repeated at each MPP tracking cycle until the MPP is accomplished $\Delta P \approx 0$.

However, the P&O algorithm has two main drawbacks: The MPP tracking speed and the efficiency in dynamic irradiance conditions [5]. First, the MPP tracking speed can be increased by using a bigger voltage step to perturb the PV array voltage, however, this will increase power loss due to oscillations around the MPP, whereas a smaller step reduces the oscillations, but it will take a longer time to reach the MPP [6]–[7]. To overcome the tradeoff between the speed and the oscillations, a variable step perturbation for P&O is proposed in [8], but it gives no remarkable improvement. An incremental conductance algorithm (IncCond) has been proposed in [9], however that is essentially the same algorithm as P&O.

The second issue is the poor tracking efficiency in dynamic conditions—rapidly changing solar irradiance. The P&O may track the MPP in the wrong direction, consequently the efficiency deteriorates. A solution for this issue has been presented in [5], where an improved version of the P&O is proposed. In [10], the authors proposed a multisampling P&O as an improvement, but it reaches MPP slowly in the start-up phase, as its principle requires to perform three iterations; increase the voltage with a fixed step, decrease it and increase it again (+-+). The work in [11] proposes a model predictive control as a solution, however, it requires extensive computation and variable inverter switching frequency.

Moreover in the paper [12], the authors proposed a ripple correlation control method to regulate the maximum power, by means of a 1st order high-pass filter, used to generate the PV power and the PV voltage ripple. Next, a first order low-pass filter is used to determine the sign of the product of power and voltage ripple, necessary as a reference voltage for the conventional dc-link voltage controller. The main drawback of this method is a slow response under sudden and large variations of the solar irradiance [13].

However, as described in Fig. 1, the main components of the topology used in this paper are a voltage source inverter, an output filter and a transformer for the isolation function. The output filter is essential, it is needed to filter out the switching

Manuscript received June 6, 2017; revised August 1, 2017; accepted November 27, 2017. Date of publication December 7, 2017; date of current version July 15, 2018. Recommended for publication by Associate Editor L. Chang. *(Corresponding author: Faicel El Aamri.)*

F. El Aamri and A. Mouhsen are with the Hassan First University, LRMI, FSTS, Settat 26000, Morocco (e-mail: f.elaamri@gmail.com; az.mouhsen@gmail.com).

H. Maker is with the Hassan First University, LISA, ESTB, Settat 26000, Morocco (e-mail: hattabmaker@gmail.com).

D. Sera, S. V. Spataru, and J. M. Guerrero are with the Department of Energy Technology, Aalborg University, Aalborg DK-9220, Denmark (e-mail: des@et.aau.dk; ssp@et.aau.dk; joz@et.aau.dk).

Color versions of one or more of the figures in this paper are available online at http://ieeexplore.ieee.org.

Digital Object Identifier 10.1109/TPEL.2017.2780858

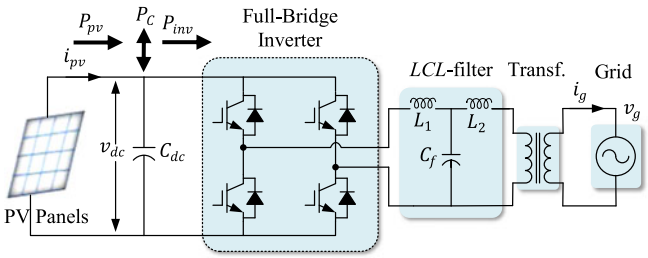

Fig. 1. System configuration of single-stage single-phase grid-connected PV system.

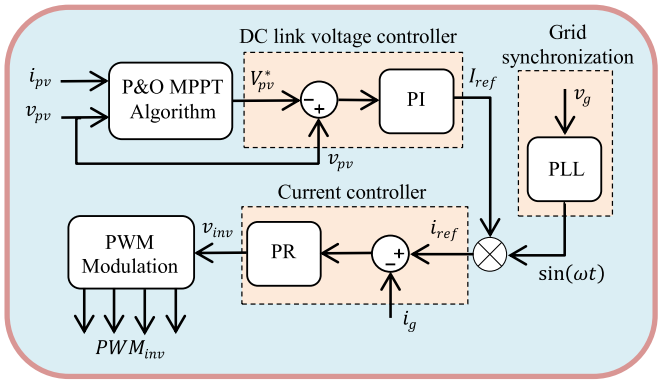

Fig. 2. Control structure for single-stage single-phase grid-connected PV inverter (PI - proportional integral, PR - proportional resonant, and PWM - pulse width modulation).

frequency harmonics. Regardless the type of the filter (L, LC, or LCL), the purpose of the output filter is to ensure the grid injected current has low total harmonic distortion and will not affect the energy transfer between the dc source and the ac grid. As for the dc-link capacitor, its main purpose is to store the energy extracted from the PV generator and smooth the dc-link voltage ripple.

In this paper, the most common control structure for this topology as shown in Fig. 2 is an MPPT algorithm [14]–[19], the dc-link voltage controller, the current controller, and the synchronization algorithm based on phase locked loop (PLL) [20]. It should be noted that the dc-link capacitor behaves as a temporary energy storage device with the amount of energy stored proportional to the dc voltage. Thus, to consider the stability of the whole controller for single-stage grid-connected PV inverter, the Lyapunov function should be formed based on the energy variation across the dc-link capacitor.

In addition, indeed all works that have been done for single-stage grid-connected PV inverters ignore to take into consideration the stability on charging and discharging the dc-link capacitor. In [21], the authors use a Lyapunov function in current controller to improve the nonlinear control, rendering the closed-loop globally asymptotically stable. In this case, the Lyapunov function is formed by the balance energy stored in the inductor and the capacitor, but the main disadvantage of this method is that it needs a more oversized system, especially the dc-link capacitor.

In this work, we propose a direct MPPT control scheme for single-phase single-stage grid-connected PV inverters that solves both P&O drawbacks: 1) ensuring a fast tracking with considerably reduced oscillations in steady-state 2) and improved efficiency under rapidly changing irradiance.

The proposed method is based on the Lyapunov function without using a generic MPPT algorithm; it uses the instantaneous PV power ripple $\tilde{P}_{\rm pv}$ and the instantaneous PV voltage ripple $\tilde{V}_{\rm pv}$ across the dc-link capacitor. The ratio of $\tilde{P}_{\rm pv}/\tilde{V}_{\rm pv}$ determines the position of the operating point on the P-V curve. Thereafter, the ratio result dP/dV is multiplied by a gain K in order to regulate the power fed into the grid.

The remainder of this paper is organized as follows: in Section II, the mathematical model of the proposed controller is presented, which is based on the Lyapunov function that is formed by the variation of the stored energy across the dc-link capacitor. In Section III, the simulation results using both methods are presented, whereas the experimental setup and results are shown in Section IV. The conclusions are presented and summarized in Section V.

II. Control Strategy

A. Power Flow Description

Considering the single-stage single-phase grid-connected photovoltaic inverter as shown in Fig. 1, and assuming no power losses in the inverter, dc-link capacitor and output filter, (so that the other terms accounting for the conduction losses can be neglected to obtain a simple expression), the equation describing the power balance in the dc link can be written as

$$P_{\rm pv}\left(t\right) = P_C\left(t\right) + P_{\rm grid}\left(t\right). \tag{1}$$

The power fed into the grid $P_{\rm grid}$ is equal to

$$P_{\rm grid}\left(t\right) = v_g i_g = V_g I_g\left(1 - \cos 2\omega t\right) \tag{2}$$

where v_g and i_g are the instantaneous grid voltage and grid current respectively. I_g is the root mean square (rms) of the injected current, V_g is the rms of the grid voltage, and ω is the grid pulsation. The power injected into single-phase grid $P_{\rm grid}$, calculated as in (2), follows a sinusoidal waveform with twice the grid frequency. The PV generator could not be operated at the MPP if this pulsating power is not decoupled by means of an energy buffer. Therefore, a capacitor bank is typically used for buffering this energy.

The $P_c(t)$ is the instantaneous power flow in the dc-link capacitor and is equal to

$$P_C\left(t\right) = C_{\rm dc} V_{\rm dc} \frac{dV_{\rm dc}}{dt}. \tag{3}$$

The average power P_{av} fed into the grid can be written as

$$P_{av} = \frac{1}{T_{\rm grid}} \int_0^{T_{\rm grid}} V_g I_g\left(1 - \cos 2\omega t\right) = V_g I_g \tag{4}$$

where $T_{\rm grid}$ is the grid voltage period.

B. Proposed Controller

The control system of the PV inverter can be divided into following three parts:

1) dc-link voltage controller;

2) current controller; and
3) grid synchronization controller.

The dc-link voltage controller is used to regulate the dc voltage at a desirable level for extracting the maximum power from the PV array. Considering that the PV characteristic is nonlinear, while the irradiance changes, the dc power will change accordingly, consequently, the MPP will also shift. In this case, since the grid voltage is fixed (this can be assumed in most cases), the power transferred to the grid is controlled only by the inverter output current.

The mathematical model describing the dynamics of the power flow is given by (5), where I_g^* represents the reference grid current of the inverter

$$V_g I_g^* = I_{\rm pv} V_{\rm pv} - C_{\rm dc} V_{\rm dc} \frac{dV_{\rm dc}}{dt} \tag{5}$$

where $V_{\rm pv}$ and $I_{\rm pv}$ are periodic signals having the average components $\bar{V}_{\rm pv}$, $\bar{I}_{\rm pv}$ and the ac components $\tilde{v}_{\rm pv}$, $\tilde{i}_{\rm pv}$ with oscillation period $T = 1/(2f_{\rm grid})$, and defined respectively as

$$\begin{cases} V_{\rm pv} = \bar{V}_{\rm pv} + \tilde{v}_{\rm pv} \\ I_{\rm pv} = \bar{I}_{\rm pv} + \tilde{i}_{\rm pv} \end{cases}. \tag{6}$$

The power injected into the grid P_{av} is controlled according to (7), using a feed-forward power $P_{\rm pv}$ term, and a second term KdP/dV accounting for the dynamics of the PV inverter system

$$P^* = P_{\rm pv} + K\frac{dP}{dV} \tag{7}$$

where $\boldsymbol{P^*}$ represents the reference power and $\boldsymbol{K}$ is a constant parameter which allows adjusting the amount of power in the controller to follow the maximum power point, and it will be discussed in detail later on. Hence, substituting (7) into (5) yields

$$V_g I_g^* = P_{\rm pv} + K\frac{dP}{dV} \tag{8}$$

and by substituting (8) into (5) we get

$$C_{\rm dc} V_{\rm dc} \frac{dV_{\rm dc}}{dt} = -K\frac{dP}{dV}. \tag{9}$$

Based on (9), we can deduce that the dP/dV is related to the dc-link capacitor dynamics.

The estimation method of the ac components (ripples) of the PV power $\tilde{p}_{\rm pv}$ and the dc-link voltage $\tilde{v}_{\rm dc}$, is based on a second-order generalized integrator-based quadrature signal generator (SOGI-QSG) [22], as presented in Fig. 3 and defined by the closed-loop transfer function in the following:

$$F(s) = \frac{\omega_n s}{s^2 + \omega_n s + {\omega_n}^2} \tag{10}$$

where ω_n represents the resonance frequency, equal to double the grid frequency.

Fig. 4 shows the proposed control strategy. The computed value of the reference current is determined using the PV Power reference generated by the proposed controller as shown in Fig. 3 and the rms value of the grid voltage. The PLL extracts the phase angle of the grid voltage and is multiplied by the magnitude

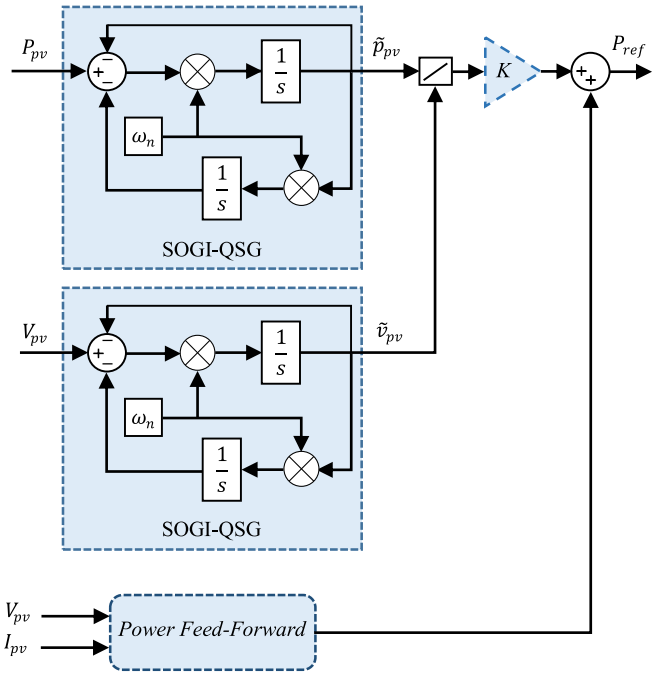

Fig. 3. Generation of reference power using SOGI-QSG.

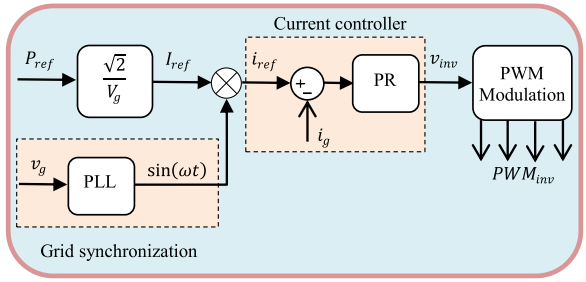

Fig. 4. Overall controller configuration using the proposed reference power as input and using unipolar PWM.

of the reference grid current. Then, the current controller is proceeding to regulate the grid current i_g.

C. Stability Analysis

The stability of the closed-loop system will be determined primarily by the sign and magnitude of the controller parameter K. In order to determine the sign of the parameter K, we use Lyapunov's stability theorem to study the overall system's stability. According to [23], the Lyapunov function $V(x)$ is a scalar energy function, the system is stable if $V(x)$ satisfies that $V(0) = 0, V(x) > 0$ for all $x \neq 0$ and $\frac{dV(x)}{dt} < 0$ for all $x \neq 0$.

To achieve this, we derive the Lyapunov function $V(E_n)$ as in (11), based on the energy variation across the dc-link capacitor, and assuming that the energy stored in the grid filter can be neglected

$$V(E_n) = \frac{C_{\rm dc}^2}{4}\left(V_{\rm dc}^{*2} - V_{\rm dc}^2\right)^2 \tag{11}$$

where E_n refers the energy stored in dc-link capacitor and $V_{\rm dc}^*$ is the reference dc-link voltage.

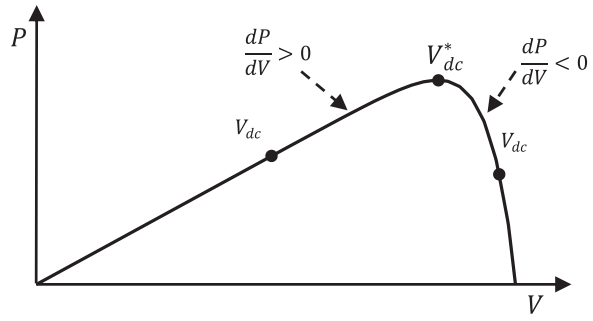

Fig. 5. Movement of the operating point on P-V characteristic.

To ensure global stability of the dynamic system, the condition $V(E_n)\dot{V}(E_n) < 0$ must hold for all $E_n \neq 0$. Consequently, $V(E_n) > 0$ and $\dot{V}(E_n) < 0$, where

$$\frac{dV\left(E_n\right)}{dt} = \frac{C_{dc}^2}{2}\left(V_{\rm dc}^{*2} - V_{\rm dc}^2\right)\left(0 - 2V_{\rm dc}\frac{dV_{\rm dc}}{dt}\right). \quad (12)$$

Finally, by arranging the terms it can be obtained as

$$\frac{dV\left(E_n\right)}{dt} = -C_{\rm dc}^2 V_{\rm dc}\frac{dV_{\rm dc}}{dt}\left(V_{\rm dc}^{*2} - V_{\rm dc}^2\right). \quad (13)$$

Therefore, to check the previous condition $V(E_n)\dot{V}(E_n) < 0$ for the controller stability and according to (13), if $V_{\rm dc} > V_{\rm dc}^*$ and $\dot{V}(E_n) < 0$, this implies that $dV_{\rm dc}/dt < 0$.

According to (9), $C_{\rm dc}V_{\rm dc}\frac{dV_{\rm dc}}{dt} < 0$, which implies that $-KdP/dV < 0$.

Therefore, since the operating point is located on the right side because it was assumed that $V_{\rm dc} > V_{\rm dc}^*$ as shown in Fig. 5, it gives $dP/dV < 0$, which means that $K < 0$.

The following equation summarizes the proof:

$$\text{if } V_{\rm dc} > V_{\rm dc}^*, \frac{dV\left(E_n\right)}{dt} < 0 \Rightarrow \frac{dV_{\rm dc}}{dt} < 0 \Rightarrow K < 0. \quad (14)$$

As for the other case, if $V_{\rm dc} < V_{\rm dc}^*$ and since $\dot{V}(E_n)$ should be negative, this implies that $dV_{\rm dc}/dt > 0$.

According to (9), $C_{\rm dc}V_{\rm dc}\frac{dV_{\rm dc}}{dt} > 0$, resulting that $-K\frac{dP}{dV} > 0$.

Therefore, since the operating point is located on the left side because it was assumed that $V_{\rm dc} < V_{\rm dc}^*$, as shown in Fig. 5, it gives that $dP/dV > 0$, which means that $K < 0$.

The following equation summarizes the proof:

$$\text{if } V_{\rm dc} < V_{\rm dc}^*, \frac{dV\left(E_n\right)}{dt} < 0 \Rightarrow \frac{dV_{\rm dc}}{dt} > 0 \Rightarrow K < 0. \quad (15)$$

However, it should be mentioned that during normal operation, the system will be subject to disturbances. The dc-link capacitor is used as a damping element to maintain the stability for the MPPT and the grid-connected inverter during these transitory states.

The dc-link capacitor is sized based on the allowable magnitude of the PV voltage ripple, therefore the PV power can be written as the equation below:

$$P_{\rm pv} = 2\pi f_{\rm grid}.C_{\rm dc}.V_{\rm dc}.\Delta V_{\rm dc}. \quad (16)$$

As shown in (16), the dc-link voltage ripple depends on the parameters; $P_{\rm pv}$ and $V_{\rm dc}$, which are related to the PV characteristic, to designate the capacitor value, it should be taken into consideration the low irradiation, in this case the PV power decreases considerably than the PV voltage, which impose to size the capacitor based on low irradiation in order to keep $\Delta V_{\rm dc}$ distinctive on the noise measurement.

As a consequence, the minimum capacitance required for this amount of the power and the dc-link voltage ripple is determined as follows:

$$C_{\rm dc} = \frac{P_{\rm pv}}{2\pi f_{\rm grid}.V_{\rm dc}.\Delta V_{\rm dc}}. \quad (17)$$

In this paper, $\Delta V_{\rm dc}$ is set to 6 V at standard test conditions (STC). In addition, the parameter K should be calculated carefully for a given system to avoid the risk of operating the system in an unstable state.

Next, we can reformulate (7) as

$$P^* = P_{\rm pv} + \Delta P^* \quad (18)$$

where ΔP^* is the power adjustment, that controls the speed to reach the maximum power point. As long as ΔP^* increases, the MPPT speed becomes faster, while the stability margin of the whole system decreases. Its expression contains two parameters, the first one is a constant K and the second one is a variable ratio dP/dV that depends on the operating point on the P-V curve.

In order to ensure the stability PV inverter system in the entire solar irradiation range (0–1000 W/m^2), as K is just a constant, we will focus on the variable ratio dP/dV.

In the vicinity of the maximum power point, the variation of P, can be expressed as

$$\tilde{P} = \Delta\left(I_{\rm MPP}V_{\rm MPP}\right) = V_{\rm MPP}\tilde{i}_{\rm pv} + I_{\rm MPP}\tilde{v}_{\rm pv} + \tilde{v}_{\rm pv}\tilde{i}_{\rm pv}. \quad (19)$$

By arranging the terms, we can get

$$\frac{\tilde{P}_{\rm pv}}{\tilde{v}_{\rm pv}} = V_{\rm MPP}\frac{\tilde{i}_{\rm pv}}{\tilde{v}_{\rm pv}} + I_{\rm MPP} + \tilde{i}_{\rm pv}. \quad (20)$$

Based on [24], it can be assumed that

$$\left.\frac{\tilde{i}_{\rm pv}}{\tilde{v}_{\rm pv}}\right|_{\rm MPP} = -\frac{I_{\rm MPP}}{V_{\rm MPP}}. \quad (21)$$

Substituting (21) into (20) we get

$$\frac{\tilde{P}_{\rm pv}}{\tilde{v}_{\rm pv}} = \tilde{i}_{\rm pv} \quad (22)$$

and by substituting (22) into (21) we get

$$\frac{\tilde{P}_{\rm pv}}{\tilde{v}_{\rm pv}} = -\frac{\tilde{v}_{\rm pv}.I_{\rm MPP}}{V_{\rm MPP}}. \quad (23)$$

In the equation above, we substitute the value of ΔV in (16), as a result we get

$$\frac{dP}{dV} = -\frac{1}{2.\pi.f_{\rm grid}.C_{\rm dc}}\frac{P_{\rm MPP}^2}{V_{\rm MPP}^3}. \quad (24)$$

According to (24), Fig. 6 shows the absolute value of dP/dV at the maximum power point for nominal power of 1 kW in each irradiance level, it can be seen that as the irradiance decreases,

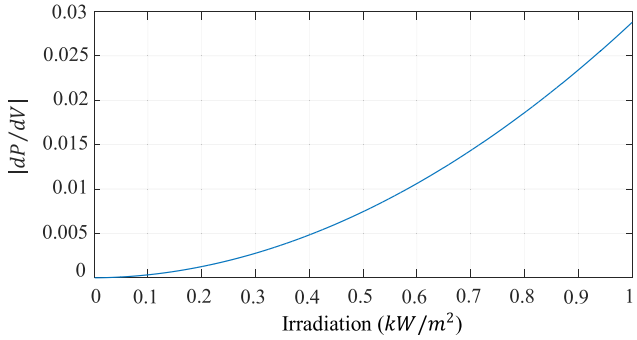

Fig. 6. Absolute value of dP/dV near MPP versus irradiance.

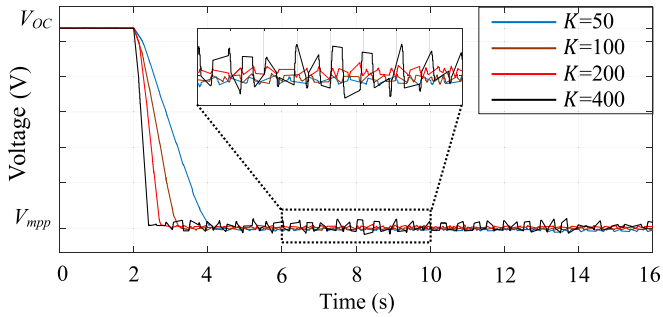

Fig. 7. Experimental PV voltage waveforms after startup showing the convergence to MPP with different K values.

the ratio decreases accordingly, owing to the more considerable drop of the PV power than the PV voltage. Which means that if the parameter K is designed for STCs at 1 kW/m^2 irradiance such that the stability criterion is fulfilled in those conditions, the system will remain stable in all lower irradiance levels, without adjusting the parameter.

On the other hand, based on (18) and (24), in the steady-state at the vicinity of the MPP, the oscillation of the PV power can be written as

$$\Delta P|_{\mathrm{MPP}} = -\frac{K}{2.\pi.f_{\mathrm{grid}}.C_{\mathrm{dc}}}\frac{P_{\mathrm{MPP}}^2}{V_{\mathrm{MPP}}^3} \tag{25}$$

which means that increasing the parameter K in the proposed controller, the MPP will be reached faster, obviously at a certain limit, increasing K does not yield significant improvements in speed, however, if K is oversized, it will cause more power oscillations, as shown in Fig. 7.

With regard to partially shaded condition, the proposed method will behave similarly to P&O, i.e., will track the nearest MPP. The advantage of this method is the fast-tracking. PS detection and tracking features (such as I-V scan) can be added in a similar manner as for the P&O. However, we consider PS detection and tracking as outside the scope of this paper, since they are not specific to the proposed method.

III. Simulation Study

The proposed control strategy has been evaluated and compared to the conventional P&O, through simulation in MATLAB/Simulink, for a single-stage single-phase grid-connected PV inverter. The parameters of PV system used in the simulation and experimental tests are summarized in the Table I.

TABLE I
Parameters for Simulation and Experiment

PV power	1 kW
V_{mpp}	455 V
I_{sc}	2.42 A
V_{oc}	568 V
DC-link capacitor	1200 μF
Switching frequency	8000 Hz
LCL-filter	$L_1 = 2.6$ mH; $C_f = 2.2$ μF; $L_2 = 0.41$ mH;
Grid nominal voltage (rms)	230 V
Grid nominal frequency	50 Hz

A. Test Case 1—Steady-State Conditions

The first test case aims to evaluate the tracking efficiency of the proposed MPPT, under standard atmospheric test constant at 1000 W/m^2 and 25 °C, respectively, at this level of the irradiance, the simulated PV array has a MPP of ∼1 kW. The parameters P&O MPPT are: $f_{\mathrm{MPPT}} = 10$ Hz—tracking frequency, and $\Delta V = 1$ V—increment step voltage, which were chosen to reduce the losses caused by permanent oscillations around the correct value of the MPP [25].

Fig. 8 shows the operation of the two MPPT control algorithms side by side. Both the proposed MPPT method (shown in red) and P&O (blue) start at time 0.4 s, which is the time when the dc-link capacitor has been completely charged, and its voltage is equal to open circuit voltage of the PV generator.

As can be observed, the proposed method reaches the MPP first and very fast, with a response time of only $t_r = 0.025$ s, compared to P&O that converges with a fixed step and a response time equal to $t_r = 11.3$ s. Moreover, we can observe that the P&O has slightly larger oscillations near the MPP voltage $V_{\mathrm{mpp}} = 455$ V- oscillating in the interval [451.5 V 459.5 V], compared to the proposed method, which oscillates in the interval [452 V 457.8 V]. From here we can conclude that the proposed MPPT method has better instantaneous efficiency in steady state than P&O. Regarding the efficiency, the P&O can also have high efficiency in steady state, however, the speed to reach the MPP will slow down.

B. Test Case 2—Dynamic Conditions

In the second test case, we analyze the dynamic efficiency of the proposed MPPT compared to P&O. This test considers a variable/trapezoidal solar irradiance profile, with a rate of change of 100 W/m^2/s, from 30% to 100% of STC irradiance, as shown in Fig. 9. Here, the black line represents the maximum power point MPP that can be generated by the PV generator. From Fig. 9, we clearly see that the change of the solar irradiance has no influence at all on the tracking efficiency for the proposed method, the black line and the red line are overlapped.

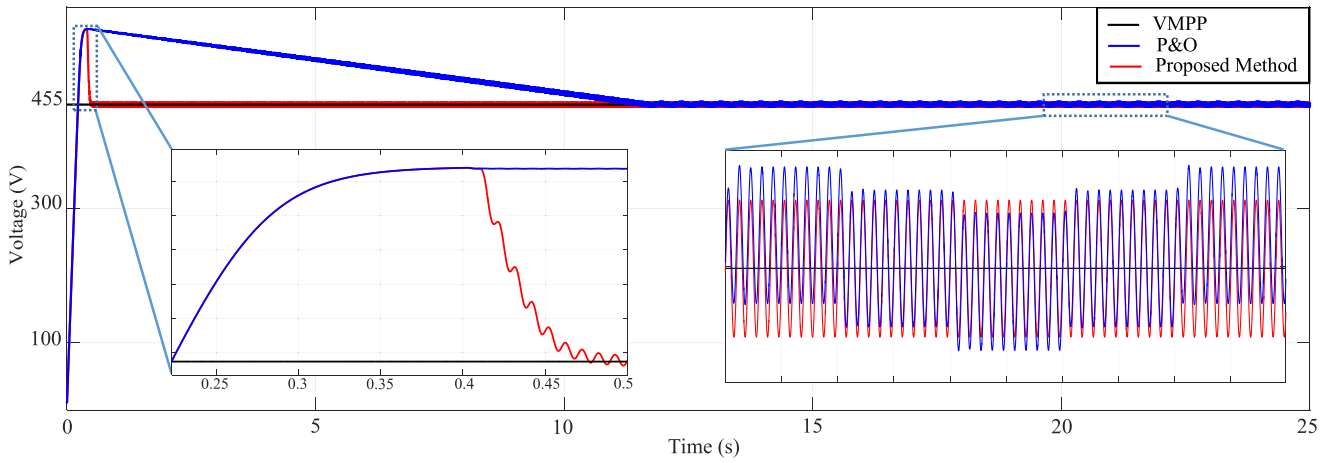

Fig. 8. Start waveforms comparison for dc-link voltage.

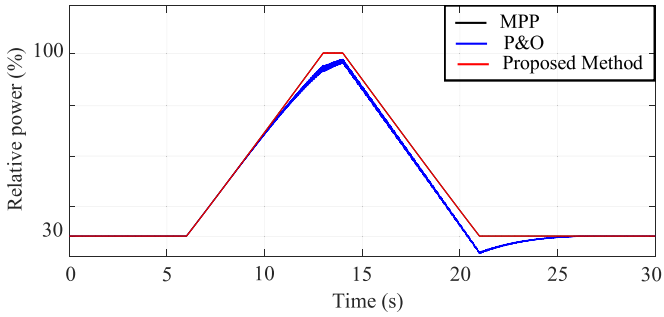

Fig. 9. Output PV power under trapezoidal irradiance profile.

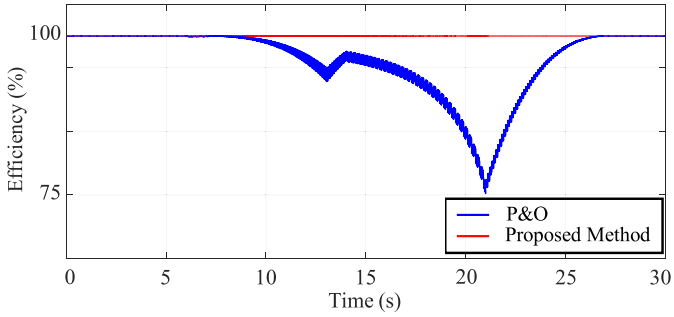

Fig. 11. Instantaneous efficiency under trapezoidal irradiance profile.

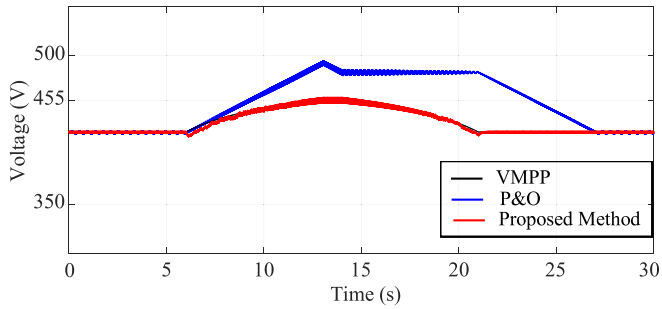

Fig. 10. DC-link voltage under trapezoidal irradiance profile.

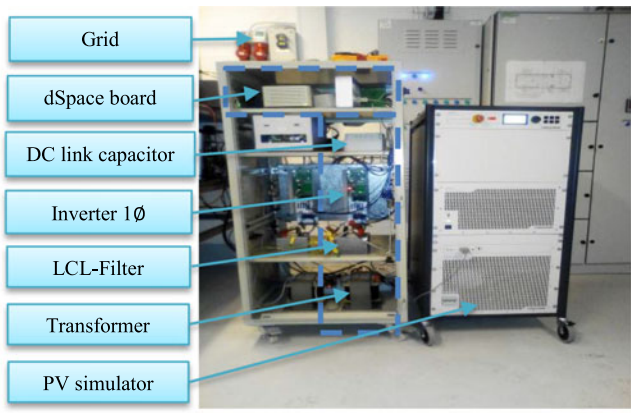

Fig. 12. Photo of the experimental setup.

As for the P&O method, we can observe in Fig. 10 that when the solar irradiance increases, the P&O cannot track the MPP accurately.

Moreover, Fig. 11 shows how the instantaneous efficiency of P&O drops about 25%, while the proposed method tracks the MPP with the same efficiency as in the steady-state operation.

IV. Experimental Validation

A. Experimental Setup Description

In the experiment study, the test setup (shown in Figs. 12 and 13) consists of the following components: 1000 V/40 A high bandwidth PV simulator (Regatron TopCon Quadro with a linear postprocessing unit TC.LIN), a 2.2 kW Danfoss VLT-FC302 inverter, grid-connected through an LCL filter, and a 1:1 single-phase transformer. The PV simulator emulates a preloaded I-V curve of the PV array. The control structure has been implemented in Simulink, and the dSPACE 1103 Real-Time Control Platform.

As shown in Fig. 13, the dSPACE controller receives the signal values measured through LEM sensors from the grid voltage, grid current, dc-link capacitor voltage, and the PV output current.

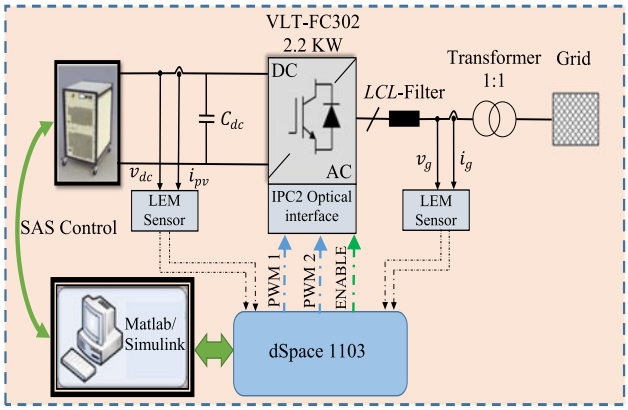

Fig. 13. Layout of the experimental setup.

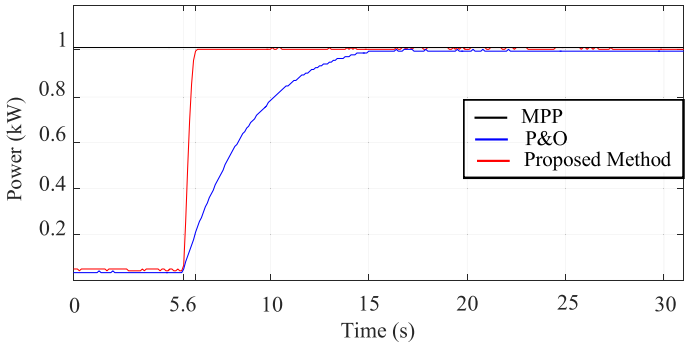

Fig. 14. Experimental start waveforms of PV power for both methods.

The parameters used for the PI voltage controller in the conventional method P&O are

$$\begin{cases} K_{p_{u-\mathrm{dc}}} = 8e^{-5} \\ K_{i_{u-\mathrm{dc}}} = 8.5e^{-4} \end{cases}. \tag{26}$$

As for the proposed method, based on (25), the parameter K is chosen equal to 200 at standard conditions.

B. Experiment Results

To verify the simulation results, different laboratory tests were carried out in the same conditions as used in the simulation. Fig. 14 shows the first experimental results that demonstrate the ability of the MPPT to reach and keep the MPP under steady-state conditions. The MPPT in both the direct reaching and P&O test case, is enabled at $t_0 = 5.6$ s. From Fig. 14, we observe that the proposed method takes ∼0.6 s to reach the MPP, while P&O takes ∼11.3 s.

Fig. 15 shows the voltage response starting at time $t_0 = 5.6$ s and $V_{\mathrm{oc}} = 568$ V.

In both cases, the MPPT reaches $V_{\mathrm{mpp}} = 455$ V but at different times. Moreover, we remark the larger oscillations around the V_{mpp} in the case of the P&O, compared to the direct MPP reaching method. These findings match the simulation results, indicating that the P&O has less instantaneous efficiency compared to the proposed method.

The second experimental test case evaluates the dynamic efficiency of two MPPs for a trapezoidal solar irradiance profile

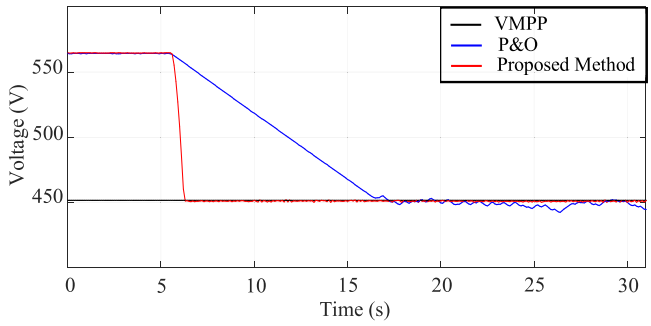

Fig. 15. Experimental start waveforms comparison of dc-link voltage.

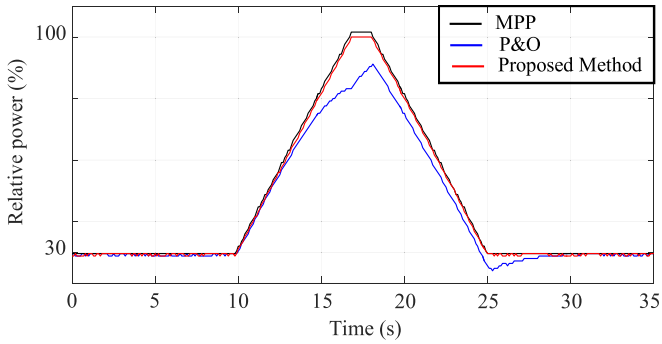

Fig. 16. Experimental results of PV power under trapezoidal irradiance profile.

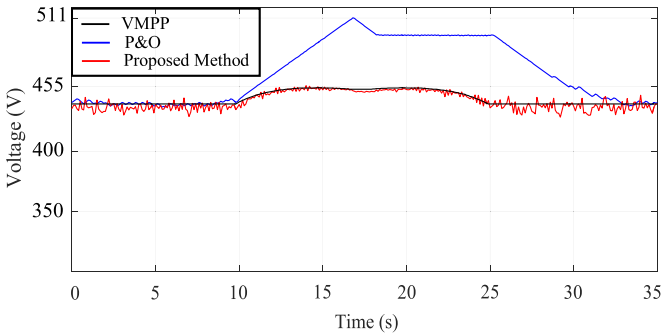

Fig. 17. Experimental results for dc-link voltage under trapezoidal irradiance profile.

with 100 W/m^2/s slope. Figs. 16 and 17 show that the proposed MPPT tracks the maximum power very well, even in dynamic conditions. By comparison, the P&O fails to track the MPP accurately, having a dynamic efficiency of $\eta = 92.97\%$, compared to the proposed MPPT of $\eta = 99.8\%$.

C. EN 50530 Test

The final experiment test aims to evaluate the MPPT efficiency according to the EN 50530 inverter test standard for static and dynamic conditions [26]. In static conditions, the EN 50530 standard evaluates the MPPT efficiency at different power levels, according to European efficiency η_{EUR} and Californian

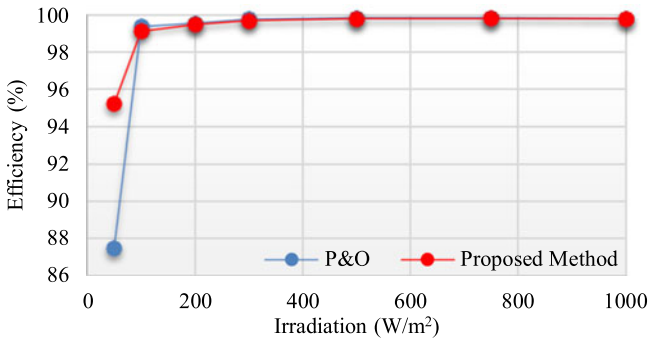

Fig. 18. Efficiency under static irradiance for both methods.

TABLE II
EXPERIMENTAL RESULTS UNDER STATIC IRRADIANCE ACCORDING TO EN 50530

	η_{EUR}	η_{CEC}
Direct MPPT	99.56	99.75
P&O	99.38	99.78

efficiency η_{CEC}:

$$\eta_{\mathrm{EUR}} = 0.03.\eta_{5\%} + 0.06.\eta_{10\%} + 0.13.\eta_{20\%} + 0.1.\eta_{30\%} + 0.48.\eta_{50\%} + 0.2.\eta_{100\%} \quad (27)$$

$$\eta_{\mathrm{CEC}} = 0.04.\eta_{10\%} + 0.05.\eta_{20\%} + 0.12.\eta_{30\%} + 0.21.\eta_{50\%} + 0.53.\eta_{75\%} + 0.05.\eta_{100\%} \quad (28)$$

where the $\eta_{5\%}$, $\eta_{10\%}$ and so on in the equations refer to MPPT efficiency at $i\%$ of STC. The equivalent static efficiencies can be calculated as below:

$$\eta_{\mathrm{stat},i} = \frac{\sum_i P_{\mathrm{PV,meas}}.\Delta T}{P_{\mathrm{mp}}.T_M} \quad (29)$$

Where $P_{\mathrm{PV,meas}}$ is the measured dc inverter power in each sampling time ΔT, P_{mp} is the maximum power of the PV array, T_M represents the whole sampling time of the measurement, and i is the power level for 5%, 10% and so on.

Fig. 18 shows the efficiency for both MPPT methods under a wide range of irradiance conditions from 50 to 1000 W/m^2. It shows that they exhibit a similar performance during high irradiance conditions, while the proposed method performance exceeds that of P&O at low irradiance levels. In this case, the PV array's power-voltage characteristic is flatter, and the P&O method becomes more sensitive to measurement noise, as a consequence, the P&O's efficiency decreases down to 87.48% for 50 W/m^2. Table II summarizes the experimental results for the proposed method and P&O. It can be seen from the comparison that the efficiencies of both methods are extremely close according to Californian efficiency η_{CEC}, while according to European efficiency η_{EUR} the proposed method is slightly better than P&O.

In the dynamic test, the MPP changes due to trapezoidal irradiance profile variation, in two sequences: 1) the first one from 10% to 50% of STC irradiance and 2) the second from the 30% to 100% of STC irradiance, as described in Tables III and IV, and as shown in Figs. 19 and 20.

TABLE III
DESCRIPTION OF THE TRAPEZOIDAL IRRADIANCE PROFILE FROM 10% TO 50% OF STC IRRADIANCE ACCORDING TO EN 50530

Sequence number	Repetition	Rise time [s]	Wait [s]	Fall time [s]	Wait [s]
1	2	80	10	80	10
2	2	40	10	40	10
3	3	20	10	20	10
4	4	13.3	10	13.3	10
5	6	8	10	8	10

TABLE IV
DESCRIPTION OF THE TRAPEZOIDAL IRRADIANCE PROFILE FROM 30% TO 100% OF STC IRRADIANCE ACCORDING TO EN 50530

Sequence number	Repetition	Rise time [s]	Wait [s]	Fall time [s]	Wait [s]
1	5	70	10	70	10
2	5	50	10	50	10
3	5	35	10	35	10
4	5	23	10	23	10
5	5	14	10	14	10
6	5	7	10	7	10

Each sequence has N repetitions of the same trapezoidal characteristic. In this case, the equivalent dynamic efficiency can be calculated as below:

$$\eta_{\mathrm{dyn}} = \frac{1}{N}\sum_{j=1}^{N}\eta_{\mathrm{dyn},j} \quad \text{where} \quad \eta_{\mathrm{dyn},j} = \frac{\sum_j P_{\mathrm{PV,meas}}.\Delta T}{\sum_j P_{\mathrm{mp}}\cdot\Delta T}. \quad (30)$$

In this paper, a shortened version of the EN 50530 dynamic test is considered, which takes around 1 h 15 min for checking completely both methods. Fig. 19 shows measured P&O tracked array power (blue) versus the real MPP of the PV array (black).

Similarly, Fig. 20 shows the tracking performance of the proposed MPPT, from where we can observe a higher dynamic efficiency (ηdyn = 99.74%), compared to P&O (ηdyn = 98.16%).

Fig. 21 summarizes the efficiency of the two MPPTs during the 5-trapezoidal from low-to-medium irradiance sequences, shown in Figs. 19 and 20. The first two sequences show similar efficiency results, with a difference between them of 0.04% approximatively due to very slow ramp speed of 80 s and 40 s, respectively. Between sequence three and fifth, the efficiency of the P&O drops because of the high speed of the ramp, with 20 s, 13.3 s, and 8 s of each of them, respectively.

Fig. 22 compares the efficiency of the two MPPTs according to the second part of the EN 50530 test, from medium-to-high irradiance. In each sequence, the proposed method exhibits an efficiency between 99.77% and 99.79%, compared to P&O which shows much lower tracking efficiency in dynamic conditions.

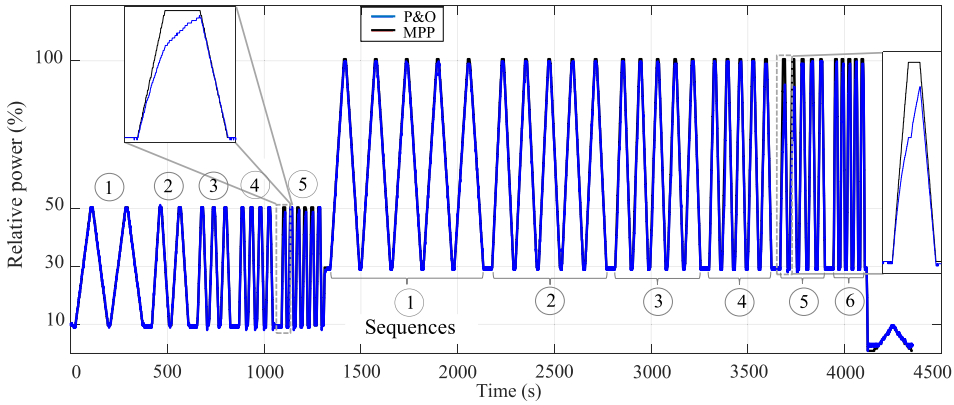

Fig. 19. PV power for P&O under dynamic irradiance profile according to EN 50530.

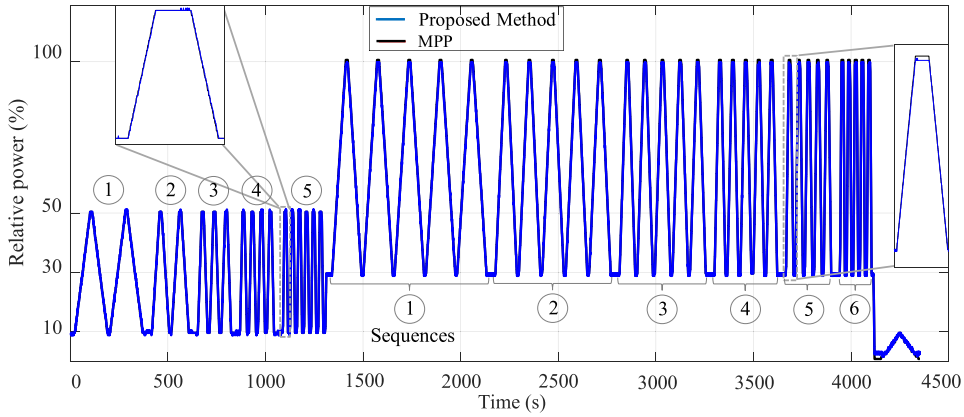

Fig. 20. PV power for the proposed method under dynamic irradiance profile according to EN 50503.

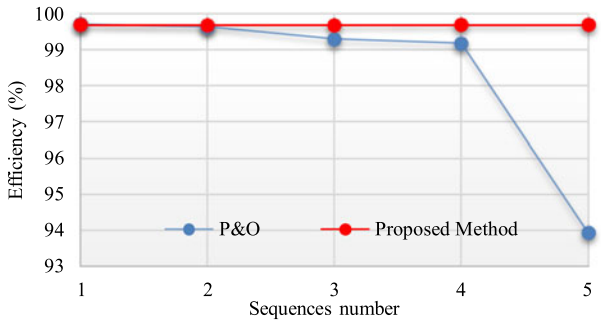

Fig. 21. Efficiency comparison for the both methods from low-to-medium irradiance.

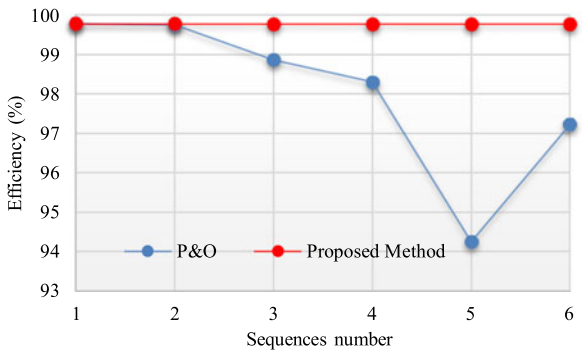

Fig. 22. Efficiency comparison for the both methods from medium-to-high irradiance.

V. Conclusion

This paper has described the design of an effective controller for direct reaching the maximum power point for a single-stage single-phase grid-connected PV inverters. The proposed method has been designed based on the stability analysis using the Lyapunov function that is formed from the variation of energy stored in the dc-link capacitor. From the simulations and experimental results on an advanced test platform and according to the EN 50530 standard, it was confirmed that the proposed method achieves high efficiency in both static and dynamic conditions. Furthermore, the proposed method is very fast to reach the MPP.

References

[1] T. Kerekes, R. Teodorescu, and U. Borup, "Transformerless photovoltaic inverters connected to the grid," in *Proc. 22nd Annu. IEEE Appl. Power Electron. Conf. Expo.*, 2007, pp. 1733–1737.

[2] I. S. Kim, M. B. Kim, and M. J. Youn, "New maximum power point tracker using sliding-mode observer for estimation of solar array current in the grid-connected photovoltaic system," *IEEE Trans. Ind. Electron.*, vol. 53, no. 4, pp. 1027–1035, Jun. 2006.

[3] J. Selvaraj and N. A. Rahim, "Multilevel inverter for grid-connected PV system employing digital PI controller," *IEEE Trans. Ind. Electron.*, vol. 56, no. 1, pp. 149–158, Jan. 2009.

[4] M. Rosu-Hamzescu and S. Oprea, *Practical Guide to Implementing Solar Panel MPPT Algorithms*. Chandler, AZ, USA: Microchip Technol. Inc, 2013.

[5] D. Sera, R. Teodorescu, J. Hantschel, and M. Knoll, "Optimized maximum power point tracker for fast-changing environmental conditions," *IEEE Trans. Ind. Electron.*, vol. 55, no. 7, pp. 2629–2637, Jul. 2008.

[6] X. Liu and L. A. C. Lopes, "An improved perturbation and observation maximum power point tracking algorithm for PV arrays," in *Proc. 2004 IEEE 35th Annu. Power Electron. Spec. Conf. (IEEE Cat. No.04CH37551)*, vol. 3, 2004, pp. 2005–2010.
[7] X. Li, H. Wen, L. Jiang, W. Xiao, Y. Du, and C. Zhao, "An Improved MPPT method for PV system with fast-converging speed and zero oscillation," *IEEE Trans. Ind. Appl.*, vol. 52, no. 6, pp. 5051–5064, Nov./Dec. 2016.
[8] S. K. Kollimalla and M. K. Mishra, "Variable perturbation size adaptive P&O MPPT algorithm for sudden changes in irradiance," *IEEE Trans. Sustain. Energy*, vol. 5, no. 3, pp. 718–728, Jul. 2014.
[9] D. Sera, L. Mathe, T. Kerekes, S. V Spataru, and R. Teodorescu, "On the perturb-and-observe and incremental conductance MPPT methods for PV systems," *IEEE J. Photovolt.*, vol. 3, no. 3, pp. 1070–1078, Jul. 2013.
[10] G. Escobar, S. Pettersson, C. N. M. Ho, and R. Rico, "Multi-sampling maximum power point tracker (MS-MPPT) to compensate irradiance and temperature changes," *IEEE Trans. Sustain. Energy*, vol. 8, no. 3, pp. 1096–1105, Jul. 2017.
[11] M. Metry, M. B. Shadmand, R. S. Balog, and H. Abu-Rub, "MPPT of photovoltaic systems using sensorless current-based model predictive control," *IEEE Trans. Ind. Appl.*, vol. 53, no. 2, pp. 1157–1167, Mar./Apr. 2017.
[12] D. Casadei, G. Grandi, and C. Rossi, "Single-phase single-stage photovoltaic generation system based on a ripple correlation control maximum power point tracking," *IEEE Trans. Energy Convers.*, vol. 21, no. 2, pp. 562–568, Jun. 2006.
[13] M. Hammami, G. Grandi, and M. Rudan, "An improved MPPT algorithm based on hybrid RCC scheme for single-phase PV systems," in *Proc. 42nd Annu. Conf. IEEE Ind. Electron. Soc.*, 2016, pp. 3024–3029.
[14] M. Ciobotaru, R. Teodorescu, and F. Blaabjerg, "Control of single-stage single-phase PV inverter," *EPE J.*, vol. 16, no. 3, pp. 20–26, Sep. 2006.
[15] F. Paz and M. Ordonez, "Zero oscillation and irradiance slope tracking for photovoltaic MPPT," *IEEE Trans. Ind. Electron.*, vol. 61, no. 11, pp. 6138–6147, Nov. 2014.
[16] J. Ahmed and Z. Salam, "A modified P&O maximum power point tracking method with reduced steady-state oscillation and improved tracking efficiency," *IEEE Trans. Sustain. Energy*, vol. 7, no. 4, pp. 1506–1515, Oct. 2016.
[17] J. H. Teng, W. H. Huang, T. A. Hsu, and C. Y. Wang, "Novel and fast maximum power point tracking for photovoltaic generation," *IEEE Trans. Ind. Electron.*, vol. 63, no. 8, pp. 4955–4966, Aug. 2016.
[18] M. Killi and S. Samanta, "An adaptive voltage-sensor-based MPPT for photovoltaic systems with SEPIC converter including steady-state and drift analysis," *IEEE Trans. Ind. Electron.*, vol. 62, no. 12, pp. 7609–7619, Dec. 2015.
[19] V. Kokaew, S. M. Sharkh, and M. Moshrefi-Torbati, "Maximum Power point tracking of a small-scale compressed air energy storage system," *IEEE Trans. Ind. Electron.*, vol. 63, no. 2, pp. 985–994, Feb. 2016.
[20] M. Ciobotaru, R. Teodorescu, and F. Blaabjerg, "A new single phase PLL structure based on second order generalized integrator," in *Proc. Power Electron. Spec. Conf.*, 2006, pp. 1–6.
[21] C. Meza, D. Biel, D. Jeltsema, and J. M. A. Scherpen, "Lyapunov-based control scheme for single-phase grid-connected PV central inverters," *IEEE Trans. Control Syst. Technol.*, vol. 20, no. 2, pp. 520–529, Mar. 2012.
[22] S. Golestan, S. Y. Mousazadeh, J. M. Guerrero, and J. C. Vasquez, "A critical examination of frequency-fixed second-order generalized integrator-based phase-locked loops," *IEEE Trans. Power Electron.*, vol. 32, no. 9, pp. 6666–6672, Sep. 2017.
[23] H. Komurcugil, N. Altin, S. Ozdemir, and I. Sefa, "An extended lyapunov-function-based control strategy for single-phase UPS inverters," *IEEE Trans. Power Electron.*, vol. 30, no. 7, pp. 3976–3983, Jul. 2015.
[24] N. Femia, G. Petrone, G. Spagnuolo, and M. Vitelli, "Optimization of perturb and observe maximum power point tracking method," *IEEE Trans. Power Electron.*, vol. 20, no. 4, pp. 963–973, Jul. 2005.
[25] H. Schmidt, B. Burger, U. Bussemas, and S. Elies, "How fast does an MPP tracker really need to be?," in *Proc. 24th Eur. Photovolt. Solar Energy Conf.*, 2009, pp. 3273–3276.
[26] M. Valentini, A. Raducu, D. Sera, and R. Teodorescu, "PV inverter test setup for european efficiency, static and dynamic MPPT efficiency evaluation," in *Proc. 2008 11th Int. Conf. Optim. Electr Electron. Equip.*, 2008, pp. 433–438.

Faicel El Aamri received the B.Sc. and M.Sc. degrees in electrical engineering from Cadi Ayyad University, Marrakesh, Morocco, in 2011 and 2013, respectively. He is currently working toward the Ph.D. degree in photovoltaic systems at Hassan First University, Settat, Morocco.

His research interests include control of grid-connected photovoltaic systems and power electronics.

Hattab Maker received the Ph.D. degree in power electronics and advanced control from the University of Technology Belfort-Montbéliard, Belfort-Montbéliard, France, in 2008.

He was working as a Research Engineer with Mitsubishi Electric, Renne, France. He is currently a Professor with Hassan First University, Morocco. His main research activities concern sustainable energy, power management, and power electronics.

Dr. Maker is the co-inventor of one US patent on "Method and an apparatus for controlling the switches of a Boost converter composed of plural bridge devices."

Dezso Sera (S'05–M'08–SM'15) received the B.Sc. and M.Sc. degrees in electrical engineering from the Technical University of Cluj-Napoca, Cluj-Napoca, Romania, in 2001 and 2002, respectively. He received the M.Sc. degree in power electronics and the Ph.D. degree in photovoltaic systems from the Department of Energy Technology, Aalborg University, Aalborg, Denmark, in 2005 and 2009, respectively.

Since 2009, he has been a program leader of the Photovoltaic Systems Research Program (www.pv-systems.et.aau.dk) at the same Department. He is currently working as an Associate Professor with the Department of Energy Technology, Aalborg University. His research interests include modeling, characterization, diagnostics, and maximum power point tracking (MPPT) of PV arrays, as well as power electronics and grid integration for PV systems.

Sergiu Viorel Spataru received the B.Sc. degree in electrical engineering in 2009, from the "Politehnica" University of Timisoara (UPT), Timisoara, Romania. He received the M.Sc. degree in wind power systems and the Ph.D. degree in characterization and diagnostic methods for PV modules and arrays from Aalborg University, Denmark, in 2011 and 2015, respectively. His current research activities include performance modeling of photovoltaic systems, reliability testing of photovoltaic modules, electroluminescence imaging, modeling and machine learning methods applied to diagnostic systems, and condition monitoring of photovoltaic systems.

Josep M. Guerrero (S'01–M'04–SM'08–F'15) received the B.S. degree in telecommunications engineering, the M.S. degree in electronics engineering, and the Ph.D. degree in power electronics from the Technical University of Catalonia, Barcelona, Spain, in 1997, 2000, and 2003, respectively.

Since 2011, he has been a Full Professor with the Department of Energy Technology, Aalborg University, Aalborg, Denmark, where he is responsible for the Microgrid Research Program (www.microgrids.et.aau.dk).

His research interests concern different microgrid aspects, including power electronics, distributed energy-storage systems, hierarchical and cooperative control, energy management systems, smart metering and the internet of things for ac/dc microgrid clusters and islanded minigrids. Recently, he has focused on maritime microgrids for ships, vessels, ferries, and seaports.

Prof. Guerrero is an Associate Editor for the IEEE TRANSACTIONS ON POWER ELECTRONICS, the IEEE TRANSACTIONS ON INDUSTRIAL ELECTRONICS, and the IEEE INDUSTRIAL ELECTRONICS MAGAZINE, and an Editor for the IEEE TRANSACTIONS ON SMART GRID and the IEEE TRANSACTIONS ON ENERGY CONVERSION.

Azeddine Mouhsen received the Ph.D. degree in instrumentation and measurements from Bordeaux University, Bordeaux, France, in 1995, and a state Ph.D. degree in physics from Moulay Ismaïl University, Meknes, Morocco, in 2001.

He is a Professor of physics with Hassan First University, Settat, Morocco, since 1996. He specializes in instrumentation and measurements, sensors, applied optics, energy transfer, and radiation-matter interactions. He has taught courses in physical sensors, chemical sensors, instrumentation, systems technology, digital electronics, and industrial data processing. He has published more than 20 papers and he is the co-inventor of several patents. He is the Director of the Laboratory of Radiation - Matter & Instrumentation, since 2014.